A Multiple Timestep Symplectic Algorithm for Integrating Close Encounters

Martin J. Duncan
Department of Physics, Queen's University, Kingston, Ontario, Canada K7L 3N6

Harold F. Levison
Space Science Department, Southwest Research Institute, Boulder, CO 80302

and

Man Hoi Lee[1]
Department of Physics, Queen's University, Kingston, Ontario, Canada K7L 3N6

ABSTRACT

We present a new symplectic algorithm that has the desirable properties of the sophisticated but highly efficient numerical algorithms known as Mixed Variable Symplectic (MVS) methods, and that in addition can handle close encounters between objects. This technique is based on a variant of the standard MVS methods, but it handles close encounters by employing a multiple timestep technique. When the bodies are well separated, the algorithm has the speed of MVS methods, and whenever two bodies suffer a mutual encounter, the timestep for the relevant bodies is recursively subdivided to whatever level is required. We demonstrate the power of this method using several tests of the technique. We believe that this algorithm will be a valuable tool for the study of planetesimal dynamics and planet formation.

Subject headings: celestial mechanics, stellar dynamics — methods: numerical — planetary systems — solar system: general

---

[1]Present address: Department of Physics, University of California, Santa Barbara, CA 93106

1. Introduction

In the last few years, the capacity of the astronomical community to perform long-term numerical orbital integrations of solar system objects has increased by a factor of over 100. This incredible increase is due in part to the availability of fast, low-cost computer workstations. More important, however, has been the development of sophisticated but highly efficient numerical algorithms known as Mixed Variable Symplectic (MVS) methods (Wisdom & Holman 1991, hereafter WH91; Saha & Tremaine 1992). With MVS methods, integrations of objects in the outer solar system on timescales approaching the age of the solar system (4.5 billion years) are now possible.

Despite their power and their many contributions, the MVS algorithms have severe limitations. In particular, none of the existing methods allows adaptive timesteps.[2] Hence the existing methods cannot handle close encounters between objects. Yet the ability to follow close encounters between objects is very important to our understanding of many of the processes that molded, and are continuing to affect, the structure of our solar system (and other planetary systems). Included in these processes are (*i*) the accumulations of the planets, (*ii*) the long-term evolution of unstable planetary and satellite systems, and (*iii*) the long-term dynamics of small bodies.

In this paper we develop a new symplectic algorithm that can integrate through close encounters between bodies. The algorithm combines a variant of the standard MVS methods with an improved version of the multiple timestep methods, originally developed by Skeel & Biesiadecki (1994; see also Biesiadecki & Skeel 1993). This new second-order method has the desirable properties of a symplectic method, and it has the speed of the MVS methods when the bodies are well separated. In § 2, we present a brief review of symplectic integrators and MVS methods. In § 3, we discuss the close encounter algorithm. In § 4, we develop a variant of the MVS methods that is used as the basis for our new algorithm. The complete new algorithm is described in § 5, and it is tested in § 6. Finally, we present our concluding remarks in § 7.

---

[2]In original form, the MVS methods require a constant timestep for all particles. A method with individual, but not adaptive, timesteps was developed by Saha & Tremaine (1994).

2. Background on Symplectic Integrators

Symplectic integrators have become popular in recent years because the Newtonian gravitational N-body problem is a Hamiltonian problem and these integrators preserve certain properties that are intrinsic to Hamiltonian systems (see Sanz-Serna & Calvo 1994 for a review). In particular:

(i) As their name implies, these integrators are symplectic, i.e., they preserve the symplectic structure $d\boldsymbol{p} \wedge d\boldsymbol{q}$, where $(\boldsymbol{q}, \boldsymbol{p})$ are the canonical phase-space coordinates. This conservation property is the generalization of the preservation of phase-space area for a two-dimensional phase space.

(ii) Symplectic integrators solve exactly a nearby "surrogate" Hamiltonian problem with $\widetilde{H} = H + H_{\rm err}$. For sufficiently small timestep τ, $\widetilde{H}$ is often well represented by an autonomous Hamiltonian (see discussion in the next paragraph). Consequently, we expect that the energy error is bounded.

(iii) Many (but not all) symplectic integrators are time reversible.

Not all of these properties apply to all symplectic integrators. For example, if the timestep is varied in any way during an integration using a symplectic integrator designed for a fixed timestep, then properties (ii) and (iii) do not necessarily apply (see, e.g., Lee et al. 1997 and references therein). If in addition the timestep is varied according to the phase-space coordinates of the bodies in the integration, property (i) is lost as well (i.e., the integration is no longer symplectic; Skeel & Gear 1992). Thus, it is not possible to resolve an encounter by simply decreasing the timestep of an integration without losing the desirable properties of a symplectic integrator.

In many cases of interest, the Hamiltonian H can be divided into several parts:

$$H = \sum_{i=0}^{N} H_i, \tag{1}$$

such that each of the individual H_i is integrable. For the remainder of this section, we take $N = 1$, although, as we discuss below, N can be arbitrarily large. There are two relevant formalisms in the literature for generating symplectic integrators from Hamiltonians of this form. In the first formalism, it is noted that the evolution of the phase-space coordinates $\boldsymbol{w} = (\boldsymbol{q}, \boldsymbol{p})$ under H for a time τ is

$$\boldsymbol{w}(\tau) = e^{\tau\{\ ,H\}}\boldsymbol{w}(0) = e^{\tau\{\ ,H_0+H_1\}}\boldsymbol{w}(0), \tag{2}$$

where $\{\ ,\ \}$ is the Poisson bracket. In this formalism, a second order scheme is constructed by approximating the above operator by a composition of operators (Ruth 1983; Forest & Ruth 1990; Yoshida 1990):

$$e^{\tau\{\ ,H_0+H_1\}} \approx e^{(\tau/2)\{\ ,H_0\}}\ e^{\tau\{\ ,H_1\}}\ e^{(\tau/2)\{\ ,H_0\}}. \tag{3}$$

The three operators on the right side of equation (3) represent an algorithm that starts with evolving the system under the influence of only H_0 for half a timestep, then evolving it for a full timestep under the influence of H_1, then another half a timestep under H_0. For a symplectic integrator constructed by a composition, it can be shown by using the Baker-Campbell-Hausdorff (BCH) identity that the integrator solves a "surrogate" autonomous Hamiltonian problem with $\widetilde{H} = H + H_{\rm err}$ (e.g., Yoshida 1993). The expression for $H_{\rm err}$ is a formal series in the timestep τ and does not converge in general, but for sufficiently small τ the errors of the integrator are well represented by the leading term(s) of the series. For the second-order scheme,

$$H_{\rm err} = \frac{\tau^2}{12}\{\{H_0, H_1\}, H_1 + \frac{1}{2}H_0\} + O(\tau^4). \tag{4}$$

In the second formalism for the development of symplectic integrators (WH91), high-frequency terms are added to the Hamiltonian H to obtain a (time-dependent) mapping Hamiltonian of the form

$$H_{\rm map} = H_0 + \Phi(t,\tau)H_1, \tag{5}$$

where τ is the timestep of the integrator and $\Phi(t,\tau)$ is a sum of periodic delta functions:

$$\Phi(t,\tau) = 2\pi \sum_{j=0}^{L-1} a_j\, \delta_{2\pi}\left[2\pi\left(t/\tau - \phi_j\right)\right]. \tag{6}$$

Here $\delta_{2\pi}(x)$ is the periodic delta function of period 2π, $\delta_{2\pi}(x) = \sum_{l=-\infty}^{+\infty} \delta(x - 2\pi l)$. So Φ is a sequence of L delta functions per timestep, with amplitudes a_j and phases $\phi_j \in [0,1)$.

At the times when $\Phi = 0$, $H_{\rm map} = H_0$, so that $H_{\rm map}$ is integrable. When Φ is not zero, then $H_{\rm map}$ is effectively H_1, which again is integrable. The integration scheme is thus a sequence of steps alternating between the evolution purely due to H_0 and the evolution purely due to H_1. If we choose $L = 1$, $a_0 = 1$, and $\phi_0 = 1/2$ (WH91), this integration scheme is second-order, and it is in fact identical to the scheme in equation (3).

We will denote the above second order symplectic integrator by

$$E_0(\tau/2)\, E_1(\tau)\, E_0(\tau/2), \tag{7a}$$

where $E_i(\tau)$ represents the evolution operator under H_i for time τ. Note that another valid second order symplectic integrator can be written as

$$E_1(\tau/2)\, E_0(\tau)\, E_1(\tau/2). \tag{7b}$$

The Hamiltonian for the gravitational N-body problem is

$$H = \sum_{i=0}^{n} \frac{|\boldsymbol{p}_i|^2}{2m_i} - \sum_{i=0}^{n-1} \sum_{j=i+1}^{n} \frac{Gm_i m_j}{r_{ij}}, \tag{8}$$

where $\boldsymbol{p}_i$ is the momentum of particle i, and $r_{ij} = |\boldsymbol{q}_i - \boldsymbol{q}_j|$ is the distance between particles i and j. The simplest division of the Hamiltonian into integrable parts is to represent it as

$$H = H_T(\boldsymbol{p}) + H_V(\boldsymbol{q}), \tag{9}$$

where the $\boldsymbol{q}$'s and $\boldsymbol{p}$'s are the conjugate phase space coordinates. In this case the second-order integrator equation (7a) is

$$\begin{aligned} \tilde{\boldsymbol{p}} &= \boldsymbol{p}_\ell + \frac{\tau}{2}\boldsymbol{F}(\boldsymbol{q}_\ell), \\ \boldsymbol{q}_{\ell+1} &= \boldsymbol{q}_\ell + \tau \boldsymbol{G}(\tilde{\boldsymbol{p}}), \\ \boldsymbol{p}_{\ell+1} &= \tilde{\boldsymbol{p}} + \frac{\tau}{2}\boldsymbol{F}(\boldsymbol{q}_{\ell+1}), \end{aligned} \tag{10}$$

where $\boldsymbol{F} = -\partial H_V/\partial \boldsymbol{q}$ and $\boldsymbol{G} = \partial H_T/\partial \boldsymbol{p}$. This integrator is the familiar second-order leapfrog integrator. To achieve an accuracy of $\sim 10^{-5}$ in the energy for an integration of the solar system, this 'T+V' type second-order symplectic integrator requires a timestep $\sim 10^{-3}$ of the smallest orbital period.

However, for solar-system type integrations, a central body (the Sun) is much more massive than the other bodies in the system, and it is better to write

$$H = H_{\rm Kep} + H_{\rm int}, \tag{11}$$

where $H_{\rm Kep}$ is the part of the Hamiltonian that describes the Keplerian motion of the bodies around the central location and $H_{\rm int}$ is the part that describes the perturbation of the bodies on one another. In particular, WH91 wrote

$$H_{\rm Kep} = \sum_{i=1}^{n} \left(\frac{|\boldsymbol{p}_i'|^2}{2m_i'} - \frac{Gm_i m_0}{r_i'} \right) \tag{12}$$

and

$$H_{\rm int} = \sum_{i=1}^{n} \left(\frac{Gm_i m_0}{r_i'} - \frac{Gm_i m_0}{r_{i0}} \right) - \sum_{i=1}^{n-1} \sum_{j=i+1}^{n} \frac{Gm_i m_j}{r_{ij}}, \tag{13}$$

where r_{i0} is the distance between body i and the Sun and the primed variables refer to the Jacobi coordinates. The Jacobi coordinates can be viewed as a system where the position and momentum of each body is taken with respect to the center of mass of all bodies with lower indices (see WH91 for a formal definition). Symplectic integrators based on this division of the N-body Hamiltonian are often referred to as MVS integrators (Saha & Tremaine 1992).

Following equation (7a), a second-order MVS step involves: (i) evolving all the bodies along their Kepler orbits for time $\tau/2$; (ii) applying a kick to the momentum of each particle due to the interaction Hamiltonian (which is a function of $\boldsymbol{q}_i$ only) for time τ; (iii) again evolving all the bodies along their new Kepler orbits for time $\tau/2$. There is also a second-order scheme that is based on equation (7b).

WH91's MVS technique revolutionized the field of planetary system integration because of its speed. It has allowed integrations of a large number of particles for timescales as long as the age of the solar system (see Holman & Wisdom 1993 and Duncan et al. 1995 for examples). For well separated orbits of low eccentricity, the MVS technique gets it speed from the fact that $|H_{\rm int}| \ll |H_{\rm Kep}|$ by the ratio of the planetary mass to the solar mass, ϵ, which in turn allows the timestep of a second-order method to be increased by a factor of $\epsilon^{-1/2}$ compared to a 'T+V' leapfrog scheme. Typically, the second-order MVS methods give reasonably accurate results for timesteps on the order of 1/20 of the shortest orbital period.

Unfortunately, the MVS method loses its speed advantage when either term in $H_{\rm int}$ (eq. [13]) becomes large. Indeed, it will fail if an integration is in progress with a large τ and the magnitude of $H_{\rm int}$ grows too large. This happens in two cases: (i) The first term in $H_{\rm int}$ will get large if any body besides body 1 gets close to the Sun. This does not happen for body 1 because $r'_1 = r_{10}$ and thus the first term is always zero. (ii) The second term grows if two bodies get too close to each other.

MVS methods cannot handle close encounters between bodies while preserving their speed. Typically, users of MVS methods have been forced to stop their integrations if close encounters have occurred (e.g., Holman & Wisdom 1993; Duncan et al. 1995; Duncan & Lissauer 1997). To handle close encounters between test particles and planets, Levison & Duncan (1994) had to abandon time-reversibility and the surrogate Hamiltonian in their RMVS integrator, which uses a combination of timestep reduction and changing to planet-centered coordinates. In the next sections, we present a second-order symplectic algorithm that has the speed of MVS methods if the bodies are not involved in encounters, and that additionally can handle arbitrarily close encounters.

3. Multiple Timestep Symplectic Methods

In this section we describe a multiple timestep symplectic integrator that has all the desirable properties of the constant timestep symplectic integrators as described in § 2. This algorithm is based on ideas proposed by Skeel & Biesiadecki (1994). Some elements of our method are similar to the individual timestep scheme of Saha & Tremaine (1994).

For simplicity, let us consider first a 'T+V' integrator for the two-body Kepler problem. In this case the potential energy part of the Hamiltonian (cf. eq. [9]) is

$$H_V = -\frac{Gm_0m_1}{r}, \tag{14}$$

where $r = |\boldsymbol{q}|$ is the distance between the two bodies. The essence of our new technique in the current context is to place a series of shells around the Sun and to associate a smaller timestep with a smaller shell. As the planet approaches the Sun and crosses these shell boundaries, the timestep of the integration decreases, thereby allowing better resolution of the perihelion passage. This process must be done in such a way as to preserve the symplectic nature of the integrator. We therefore choose a set of cutoff radii $R_1 > R_2 > \cdots$ and decompose H_V into $\sum_k V_k$, or equivalently the force $\boldsymbol{F}$ into $\sum_k \boldsymbol{F}_k = -\sum_k \partial V_k/\partial \boldsymbol{q}$, such that:

(i) $\boldsymbol{F}(r) = \sum_{k=0}^{\infty} \boldsymbol{F}_k(r)$ for all r,

(ii) $\boldsymbol{F}_k$ (except $\boldsymbol{F}_0$) is zero at $r > R_k$, and

(iii) $\boldsymbol{F}_k$ is "softer" than $\boldsymbol{F}_{k+1}$ (see, e.g., Fig. 1).

We now choose a different timestep for each term in this series over V_k. In particular, the force $\boldsymbol{F}_k$ is to be applied with a timestep τ_k. In addition, τ_k/τ_{k+1} must be an integer. In general this integer can be a function of k, but in this implementation we set it to a constant, M.

With the Hamiltonian in the form

$$H = H_T + \sum_{k=0}^{\infty} V_k, \tag{15}$$

we can apply the second-order symplectic integrator in equation (7a) recursively to obtain the following second-order algorithm:

$$\begin{aligned} E_{\Sigma_0}(\tau_0) &\approx E_0(\tau_0/2)E_{\Sigma_1}(\tau_0)E_0(\tau_0/2) \\ &\approx E_0(\tau_0/2)[E_1(\tau_1/2)E_{\Sigma_2}(\tau_1)E_1(\tau_1/2)]^M E_0(\tau_0/2) \\ &\vdots \end{aligned} \tag{16}$$

where $E_i(\tau)$ and $E_{\Sigma_i}(\tau)$ denote the evolution of the phase-space coordinates under V_i and $H_T + \sum_{k=i}^{\infty} V_k$, respectively, for a timestep τ. The first line in equation (16) is simply an application of the second-order scheme in equation (7a), with the evolution under V_0 as the outer half-steps. At each level i of the recursion, the evolution under $H_T + \sum_{k=i}^{\infty} V_k$, i.e., $E_{\Sigma_i}(\tau_{i-1})$, is approximated by M second-order steps of length τ_i, with E_i as the outer half-steps.

In principle, the number of recursion levels is infinite; however, in practice, the recursion is always truncated. This is due to the fact that if $r > R_{n+1}$ then for $k > n$, $\boldsymbol{F}_k = 0$ and E_k is the identity operator. Therefore, $E_{\Sigma_{n+1}}(\tau_n)$ simply reduces to $E_T(\tau_n)$, where E_T is the evolution under H_T, and the recursion terminates. In particular, if $r > R_1$ during the entire step of length τ_0, this algorithm reduces to the standard leapfrog integrator. As r decreases, the forces are better and better resolved. However, it is important to note that although the timestep appears to vary, the high frequency terms are in principle always there, but have no effect if the associated E_k's are the identity operators. Therefore, this method is a fixed timestep symplectic algorithm and has all the properties listed in § 2.

Let us now discuss how to decompose the potential $H_V = -1/r$ into $\sum_k V_k$ (we drop the factor Gm_0m_1 for now) or equivalently the force $\boldsymbol{F}$ into $\sum_k \boldsymbol{F}_k = -\sum_k \partial V_k/\partial \boldsymbol{q}$. There are additional conditions that V_k and $\boldsymbol{F}_k$ must satisfy, and they can be deduced by examining the "error" Hamiltonian $H_{\rm err}$. For the multiple timestep algorithm (16), we can derive $H_{\rm err}$ by using the BCH identity recursively. The result can be simplified by noting that $\{V_k, V_\ell\} = 0$, and it is (cf. eq. [4])

$$H_{\rm err} = \sum_{k=0}^{\infty} \frac{\tau_k^2}{12} \{\{V_k, H_T\}, H_T + \frac{1}{2} V_k + \sum_{\ell=k+1}^{\infty} V_\ell\} + O(\tau_k^4). \tag{17}$$

It is essential that at least the lowest order [i.e., $O(\tau_k^2)$] terms in $H_{\rm err}$ are well defined. Since the lowest order terms involve nested Poisson brackets (and hence the second derivatives of V_k), V_k should at least have smooth second derivatives (and $\boldsymbol{F}_k$ smooth first derivatives). Similarly, if we want the next order [i.e., $O(\tau_k^4)$] terms in $H_{\rm err}$ to be well defined, V_k must have smooth fourth derivatives. Another condition that $\boldsymbol{F}_k$ must satisfy concerns the rate at which $|\boldsymbol{F}_k|$ decreases with decreasing r at $r \ll R_k$. As can be shown from equation (17), the number of non-zero terms in $H_{\rm err}$ increases with decreasing r. Thus, in order to ensure that the energy error does not increase rapidly with decreasing r, we want the magnitude of the kth term in equation (17) to decrease with r at $r \ll R_k$. If we assume that $|\boldsymbol{F}_k| \sim r^\alpha$ at $r \ll R_k$, a simple scaling argument using equation (17) shows that α must be > 2. We have confirmed through experimentation that both of the conditions discussed here are required. (As we shall see, for the SyMBA algorithm described in § 5, V_k and $\boldsymbol{F}_k$ must satisfy the same conditions.)

After some experiments, we have found two approaches to potential/force decomposition that work well. In both cases, it is convenient to write

$$H_V = \sum_{k=0}^{\infty} V_k = \tilde{V}_0 + (\tilde{V}_1 - \tilde{V}_0) + (\tilde{V}_2 - \tilde{V}_1) + \cdots, \tag{18}$$

so that $V_0 = \tilde{V}_0$ and $V_k = \tilde{V}_k - \tilde{V}_{k-1}$ for $k \neq 0$, and to define $\widetilde{\boldsymbol{F}}_k = -\partial \tilde{V}_k / \partial \boldsymbol{q}$.

One approach is an improved version of the method suggested by Skeel & Biesiadecki (1994). For each $\tilde{V}_{k-1}$, we let $\tilde{V}_{k-1} = -1/r$ at $r \geq R_k$ and match it to a truncated Taylor expansion of $-1/r$ at $r < R_k$. If we write $r/R_k = s^{1/n}$ and expand the potential $-1/r = -s^{-1/n}/R_k$ as a Taylor series in s at $s = 1$, then at $r < R_k$

$$\tilde{V}_{k-1} = \frac{-1}{R_k} \left\{ 1 + \frac{1}{n} \left[1 - \left(\frac{r}{R_k} \right)^n \right] + \frac{n+1}{2!\, n^2} \left[1 - \left(\frac{r}{R_k} \right)^n \right]^2 + \cdots \right\}, \tag{19}$$

and

$$\widetilde{\boldsymbol{F}}_{k-1} = - \left\{ 1 + \frac{n+1}{n} \left[1 - \left(\frac{r}{R_k} \right)^n \right] + \cdots \right\} \left(\frac{r}{R_k} \right)^{n-2} \frac{\boldsymbol{q}}{R_k^3}. \tag{20}$$

If we truncate the Taylor series in equation (19) after the ℓth order term, $\tilde{V}_{k-1}$ is smooth up to the ℓth derivatives, and $|\widetilde{\boldsymbol{F}}_{k-1}| \propto r^{n-1}$ at $r \ll R_k$. The two types of decomposition used by Skeel & Biesiadecki (1994) have $\ell = 1$ and either *i*) $n = 1$ or *ii*) $n = 2$, and they do not satisfy the minimal conditions discussed above. To satisfy the minimal conditions, we need $\ell = 2$ and $n = 4$ and

$$\widetilde{\boldsymbol{F}}_{k-1} = \begin{cases} -\boldsymbol{q}/r^3 & \text{if } r \geq R_k, \\ -\left[9 - 5(r/R_k)^4 \right] (r/R_k)^2 \boldsymbol{q}/4R_k^3 & \text{if } r < R_k. \end{cases} \tag{21}$$

If a smoother force is required, we can choose $\ell = n = 4$ and

$$\widetilde{\boldsymbol{F}}_{k-1} = - \left[663 - 1105 \left(\frac{r}{R_k} \right)^4 + 765 \left(\frac{r}{R_k} \right)^8 - 195 \left(\frac{r}{R_k} \right)^{12} \right] \left(\frac{r}{R_k} \right)^2 \frac{\boldsymbol{q}}{128 R_k^3} \tag{22}$$

if $r < R_k$. Note that these forces can be evaluated efficiently at $r < R_k$ because they involve only powers of r^2.

An alternative approach is to multiply the force by a partition function so that $|\widetilde{\boldsymbol{F}}_{k-1}|$ decreases smooth from $1/r^2$ at $r > R_k$ to zero at $r < R_{k+1}$:

$$\widetilde{\boldsymbol{F}}_{k-1} = \begin{cases} -\boldsymbol{q}/r^3 & \text{if } r \geq R_k \ , \\ -f_\ell\left(\frac{R_k - r}{R_k - R_{k+1}} \right) \boldsymbol{q}/r^3 & \text{if } R_{k+1} \leq r < R_k \ , \\ 0 & \text{if } r < R_{k+1} \ . \end{cases} \tag{23}$$

The simplest partition function $f_\ell(x)$ is the $(2\ell+1)$th order polynomial in x that has $f_\ell(0) = 1$, $f_\ell(1) = 0$, and all derivatives up to the ℓth derivative zero at $x = 0$ and 1. (In principle,

$\widetilde{\boldsymbol{F}}_{k-1}$ must be derivable from a potential $\widetilde{V}_{k-1}$; this is always true if f_ℓ is a function of only the magnitude of $\boldsymbol{q}$, r, but not its direction.) Since $\widetilde{\boldsymbol{F}}_{k-1} = 0$ at $r < R_{k+1}$, this decomposition automatically satisfies one of the minimal conditions discussed above. To satisfy the smoothness requirement, we can choose $\ell = 1$ and $f_1(x) = 2x^3 - 3x^2 + 1$. If a smoother force is required, we can choose $\ell = 3$ and $f_3(x) = 20x^7 - 70x^6 + 84x^5 - 35x^4 + 1$.

For the remainder of this paper we adopt equation (23) with $\ell = 1$. We developed this force law first and it has been tested the most thoroughly. The forces derived from this force law are shown in Figure 1. It should be noted, however, that at least in some cases the force law given in equation (22) gives slightly better behavior and appears to be just as stable. However, this force law would need to be better tested before we can recommend it over the one in equation (23).

We have implemented the multiple timestep '$T+V$' method for the two-body Kepler problem, and tests confirmed that this method has the expected properties (see Lee et al. 1997). This method can easily be extended to handle more bodies. In general, for the gravitational N-body problem,

$$H_V = -\sum_{i=0}^{n-1} \sum_{j=i+1}^{n} \frac{G m_i m_j}{r_{ij}} = \sum_{i=0}^{n-1} \sum_{j=i+1}^{n} V_{ij}. \tag{24}$$

Each term can be divided using the technique discussed above so that

$$H_V = \sum_{i=0}^{n-1} \sum_{j=i+1}^{n} \sum_{k=0}^{\infty} V_{ijk}. \tag{25}$$

In this case, each ij force pair is handled independently. Thus, if an encounter occurs between a pair of particles, the force for that pair and only that pair is sampled on a shorter timescale.

In principle, an integrator can be constructed that combines the MVS method of WH91 with the multiple timestep technique described in this section. Note that the second term in the interaction Hamiltonian of the MVS method (eq. [13]) is of the same form as the potential Hamiltonian of the '$T+V$' method (eq. [24]). Thus it is possible to subdivide the second term in the interaction Hamiltonian in the same manner (eq. [25]). In this case, the method is the same as the MVS method far from encounters and thus has its speed advantage. As two bodies enter an encounter, however, the high frequency force terms become non-zero and the timestep of the integrator is effectively decreased.

In practice, we find that this multiple timestep MVS integrator fails to behave properly for close encounters. Note from equation (12) that, because of the use of Jacobi coordinates and Jacobi masses, each body revolve about a different center with a different "effective"

central mass in the Kepler part of this algorithm. This difference is compensated for by the first term in $H_{\rm int}$ (eq. [13]). Due to the nature of our multiple timestep algorithm, $H_{\rm Kep}$ is applied at high frequency during an encounter, whereas the first term in $H_{\rm int}$ is applied at its original low frequency. Therefore, they no longer compensate each other sufficiently accurately and thus the integrator fails. A new integration method, related to the MVS method, is required to solve this problem. Such an integrator is developed in the next section.

4. Democratic Heliocentric Method

The solution to the failure of the multiple timestep MVS algorithm is to develop a variant of the standard MVS method that has all the bodies orbiting around the same central body, with the same central mass, in the Kepler part of the algorithm. In order to start the development of this new technique, we define, as we did above, $\boldsymbol{q}_i$ and $\boldsymbol{p}_i$ as the position and momentum of body i. Then the Hamiltonian (eq. [8]) is

$$H(\boldsymbol{q}_i, \boldsymbol{p}_i) = \sum_{i=0}^{n} \frac{|\boldsymbol{p}_i|^2}{2m_i} - \sum_{i=0}^{n-1} \sum_{j=i+1}^{n} \frac{G m_i m_j}{|\boldsymbol{q}_i - \boldsymbol{q}_j|}, \tag{26}$$

where body $i = 0$ is the Sun. We wish to define a new set of conjugate coordinates, $\boldsymbol{Q}_i$ and $\boldsymbol{P}_i$, so that the new positions are the heliocentric positions (if $i \neq 0$) and the position of the center of mass (if $i = 0$):

$$\boldsymbol{Q}_i = \begin{cases} \boldsymbol{q}_i - \boldsymbol{q}_0 & \text{if } i \neq 0 \\ \frac{1}{m_{\rm tot}} \sum\limits_{j=0}^{n} m_j \boldsymbol{q}_j & \text{if } i = 0 \end{cases}, \tag{27}$$

where $m_{\rm tot} = \sum_{j=0}^{n} m_j$ is the total mass. So we use a generating function of the new positions and old momenta (see, e.g., Szebehely 1967):

$$\begin{aligned} W_3(\boldsymbol{Q}_i, \boldsymbol{p}_i) &= -\boldsymbol{p}_0 \cdot \left(\boldsymbol{Q}_0 - \frac{1}{m_{\rm tot}} \sum_{j=1}^{n} m_j \boldsymbol{Q}_j \right) \\ &\quad - \sum_{i=1}^{n} \boldsymbol{p}_i \cdot \left(\boldsymbol{Q}_i + \boldsymbol{Q}_0 - \frac{1}{m_{\rm tot}} \sum_{j=1}^{n} m_j \boldsymbol{Q}_j \right). \end{aligned} \tag{28}$$

The new coordinates are canonical if

$$\boldsymbol{q}_i = -\frac{\partial W_3}{\partial \boldsymbol{p}_i} = \begin{cases} \boldsymbol{Q}_i + \boldsymbol{Q}_0 - \frac{1}{m_{\rm tot}} \sum\limits_{j=1}^{n} m_j \boldsymbol{Q}_j & \text{if } i \neq 0 \\ \boldsymbol{Q}_0 - \frac{1}{m_{\rm tot}} \sum\limits_{j=1}^{n} m_j \boldsymbol{Q}_j & \text{if } i = 0 \end{cases}, \tag{29}$$

and

$$\boldsymbol{P}_i = -\frac{\partial W_3}{\partial \boldsymbol{Q}_i} = \begin{cases} \boldsymbol{p}_i - \frac{m_i}{m_{\rm tot}} \sum\limits_{j=0}^{n} \boldsymbol{p}_j & \text{if } i \neq 0 \\ \sum\limits_{j=0}^{n} \boldsymbol{p}_j & \text{if } i = 0 \end{cases}. \tag{30}$$

Thus the new canonical momenta are the barycentric momenta (if $i \neq 0$) and the total momentum of the system (if $i = 0$). The Hamiltonian becomes

$$H(\boldsymbol{Q}_i, \boldsymbol{P}_i) = \sum_{i=1}^{n} \left(\frac{|\boldsymbol{P}_i|^2}{2m_i} - \frac{G m_i m_0}{|\boldsymbol{Q}_i|} \right)$$

$$+\frac{|\boldsymbol{P}_0|^2}{2m_{\rm tot}} + \frac{1}{2m_0}\left|\sum_{i=1}^{n}\boldsymbol{P}_i\right|^2 - \sum_{i=1}^{n-1}\sum_{j=i+1}^{n}\frac{Gm_im_j}{|\boldsymbol{Q}_i-\boldsymbol{Q}_j|}. \tag{31}$$

As expected, the center of mass ($i = 0$) moves as a free particle, and its contribution to the Hamiltonian can be ignored. Thus $H(\boldsymbol{Q}_i, \boldsymbol{P}_i) = H_{\rm Kep} + H_{\rm Sun} + H_{\rm int}$, where

$$H_{\rm Kep} = \sum_{i=1}^{n}\left(\frac{|\boldsymbol{P}_i|^2}{2m_i} - \frac{Gm_im_0}{|\boldsymbol{Q}_i|}\right), \tag{32a}$$

$$H_{\rm Sun} = \frac{1}{2m_0}\left|\sum_{i=1}^{n}\boldsymbol{P}_i\right|^2, \tag{32b}$$

$$H_{\rm int} = -\sum_{i=1}^{n-1}\sum_{j=i+1}^{n}\frac{Gm_im_j}{|\boldsymbol{Q}_i-\boldsymbol{Q}_j|}. \tag{32c}$$

We denote the part of the Hamiltonian in equation (32b) as $H_{\rm Sun}$ because $-\sum_{i=1}^{n}\boldsymbol{P}_i = \boldsymbol{p}_0 - (m_0/m_{\rm tot})\sum_{i=0}^{n}\boldsymbol{p}_i$ is the barycentric momentum of the Sun.

For the above Hamiltonian, we can construct a second-order single timestep symplectic integrator of the form

$$E_{\rm Sun}(\tau/2)\, E_{\rm int}(\tau/2)\, E_{\rm Kep}(\tau)\, E_{\rm int}(\tau/2)\, E_{\rm Sun}(\tau/2). \tag{33}$$

(Since $\{H_{\rm Sun}, H_{\rm int}\} = 0$, the ordering of $E_{\rm Sun}$ and $E_{\rm int}$ does not affect the result.) The algorithm is thus: (*i*) Each body takes a linear drift in position of the amount $\frac{\tau}{2m_0}\sum \boldsymbol{P}_i$. (*ii*) Each body receives a kick to its momentum due to the gravitational force of the other bodies (except the Sun) in the system for $\tau/2$. (*iii*) Each body evolves along a Kepler orbit for time τ. (*iv*) Each body again receives a kick to its momentum for $\tau/2$. (*v*) Each body again takes a linear drift in position.

Figure 2 shows a comparison between the standard MVS method and this new method, where we integrated the 4 outer planets of the solar system using both techniques with a timestep of 0.4 years. The top panel of the figure shows the fractional change in the energy of the system as a function of time in the MVS integration. Notice that it has the desired characteristic of a symplectic integrator that the energy error is bounded. The bottom panel shows the same quantity for the integration using the new algorithm. The energy error is also bounded in this case. In addition, the magnitude of the energy variations in the two runs are very similar, both having an rms variation $\sim 5 \times 10^{-8}$ about the mean.

This new method has several advantages and disadvantages over the standard MVS method. It has the desired characteristic, discussed at the beginning of this section, that

all the objects revolve about the same central location with the same central mass in the Kepler part of the algorithm. (In addition, the $E_{\rm Sun}$ parts do not change the relative position $\boldsymbol{Q}_i - \boldsymbol{Q}_j$ between two bodies.) This will allow us to apply the multiple timestep algorithm presented in the last section. Since the central mass is the same for all bodies and the positions are the heliocentric ones, we call this method the *Democratic Heliocentric* or DH method.[3]

Another important advantage of the DH method is that while the ordering of the bodies is important in the MVS scheme, it is not in the DH method. Recall from § 2 that the Kepler part of the MVS integrator is based on the Jacobi coordinates. Recall also that the Jacobi coordinates are a system where the position and momentum of each body is taken with respect to the center of mass of all bodies with lower indices. The formal definition of the Jacobi coordinates does not specify a particular ordering of the bodies, and it is possible to order them so that, for example, in a system with two planets, the outer planet's $\boldsymbol{q}'$ and $\boldsymbol{p}'$ are taken with respect to the Sun, while the inner planet's are taken with respect to the center of mass of the Sun and the outer planet. However, with such an ordering, the energy conservation of the MVS algorithm is significantly degraded (see also Chambers & Wetherill 1998). It is much better to order the bodies so that increasing indices correspond to increasing semi-major axes.

This ordering becomes problematic when we consider a system of massive bodies on crossing orbits, such as in planet formation simulations. In this case, objects will experience large changes in their semi-major axes due to close encounters. Thus, the appropriate ordering for the MVS integrator, which is based on semi-major axes, will not be the same for all time. Unfortunately, it is not possible to reorder the particles, because this changes the surrogate Hamiltonian associated with the integration. Therefore, any close encounter algorithm that is based on the MVS method can have significant problems, even if the encounters are accurately integrated. Fortunately, the DH method does not suffer from this problem.

The largest disadvantage of the DH method is that it does not handle orbits with small pericentric distances very well. This is best illustrated by considering the Kepler problem. The top panel of Figure 3 shows the maximum fractional energy error in a system with the Sun and Jupiter as a function of Jupiter's perihelion distance. Jupiter was initially at aphelion, and the system was integrated for 3×10^5 years with a timestep of 0.15 years

[3]Touma & Wisdom (1994) also used the coordinates $\boldsymbol{Q}_i$ and $\boldsymbol{P}_i$ in their Lie-Poisson integrators, which are extensions of the MVS integrators for rigid body dynamics. However, they moved terms of the form $|\boldsymbol{P}_i|^2/2m_0$ from $H_{\rm Sun}$ to $H_{\rm Kep}$. This grouping results in different central masses in the Kepler part of the algorithm and different linear drifts in the $E_{\rm Sun}$ parts.

(i.e., ≈ 79 steps per orbit). The MVS method can integrate the Kepler problem to machine precision (independent of timestep) because the interaction Hamiltonian is zero in this case (see eq. [13]). This degeneracy does not happen in the DH method. As equation (32) shows, although $H_{\rm int} = 0$ in the Kepler problem, $H_{\rm Sun}$ is not. This is due to the fact that the conjugate coordinates in this integrator are the heliocentric positions and the *barycentric* momenta. So, even in the Kepler problem, the Kepler part of the DH method (eq. [32a]) does not represent the orbit exactly, and $H_{\rm Sun}$ is needed as a correction. The error grows as $H_{\rm Sun}$ (or $|\boldsymbol{P}_1|$) becomes large, which happens if the planet gets close to the Sun. Therefore, the error of the integrator increases with decreasing pericentric distance, as seen in the figure.

We should note, however, that the MVS method can only handle small pericentric distances for massless particles and the *innermost* planet (if they have the lowest indices). For a massive body that is not the innermost planet, the first term in $H_{\rm int}$ is not identically zero. Thus, the MVS method will fail if one of these objects comes too close to the Sun. As an example, we integrated a system consisting of the Sun, Jupiter, and Saturn. We set Saturn's inclination (relative to Jupiter) to 90°, and varied its eccentricity $e_{\rm Saturn}$. In order to avoid close encounters between the planets, if $e_{\rm Saturn} < 0.6$, we set the argument of the perihelion of Saturn to 90°. In this geometry, Saturn's perihelion and aphelion passages occur perpendicular to Jupiter's orbit. In addition, we set the argument of the perihelion of Saturn to 0° if $e_{\rm Saturn} > 0.6$. Each integration lasted for 3000 years and had a timestep of 0.15 years. The bottom panel of Figure 3 shows the maximum fractional energy error in this system as a function of Saturn's perihelion distance. The solid and dashed curves show the results for the DH and MVS integrations, respectively. For both integration techniques, energy conservation degrades as Saturn's pericentric distance decreases. For orbits with $q_{\rm Saturn} \lessapprox 2.5\,{\rm AU}$, the DH method outperforms the MVS method. Indeed, the DH method conserves energy about an order of magnitude better than the MVS method in this case.

We wish to emphasize that our intent is not to condemn the MVS technique, which has been used extensively in planetary dynamics for several years. The MVS method is excellent for the problems to which it has been applied in the past, i.e., problems with the planets on non-crossing orbits and massless particles. However, our goal in this paper is to develop a technique for studying, among other things, the late stages of planet formation, where massive bodies can be on eccentric, crossing orbits. For this case, the DH method is clearly superior to the MVS method.

5. SyMBA

We can now combine the DH method described in § 4 with the multiple timestep technique described in § 3 to construct a second-order symplectic integrator that is capable of handling close encounters. It is straightforward to apply the multiple timestep technique, because the interaction Hamiltonian $H_{\rm int}$ of the DH method (eq. [32c]) is the same as the potential Hamiltonian of the '$T+V$' method (eq. [24]) and can be replaced by $\sum V_{ijk}$ in the same manner (eq. [25]). This new algorithm has the speed of the MVS method when encounters are not taking place, and its timestep is effectively decreased during an encounter. We call this new method the *Symplectic Massive Body Algorithm* or SyMBA.

SyMBA is a time-reversible symplectic algorithm, and it has all the desirable properties listed in § 2. In particular, SyMBA has a surrogate Hamiltonian $\widetilde{H} = H + H_{\rm err}$. As in the case of the multiple timestep '$T+V$' method (see § 3), the error Hamiltonian $H_{\rm err}$ can be derived by using the BCH identity recursively. If we define

$$V_k = \sum_{i=1}^{n-1} \sum_{j=i+1}^{n} V_{ijk}, \tag{34}$$

and use the fact that $\{V_k, V_\ell\} = \{H_{\rm Sun}, V_k\} = \{\{H_{\rm Sun}, H_{\rm Kep}\}, V_k\} = 0$,

$$\begin{aligned} H_{\rm err} &= \frac{\tau_0^2}{12}\{\{H_{\rm Sun}, H_{\rm Kep}\}, H_{\rm Kep} + \frac{1}{2}H_{\rm Sun}\} \\ &\quad + \sum_{k=0}^{\infty} \frac{\tau_k^2}{12}\{\{V_k, H_{\rm Kep}\}, H_{\rm Kep} + \frac{1}{2}V_k + \sum_{\ell=k+1}^{\infty} V_\ell\} + O(\tau_k^4). \end{aligned} \tag{35}$$

The first term is associated with the $H_{\rm Sun}$ part of the algorithm, and the second term is associated with the interactions between the bodies. The existence of this error Hamiltonian is very useful because it can be used to understand some of the test results presented in this paper and to guide us in the choice of integration parameters. For example,

(i) Because of the similarity between equation (17) and the second term in equation (35), an analysis similar to that in § 3 shows that the potential V_{ijk} must satisfy the same conditions listed in § 3.

(ii) Using equation (35), we can also confirm analytically that, for the Kepler problem, the energy error increases with decreasing pericentric distance, as shown in the upper panel of Figure 3. (Note that for the Kepler problem the second term in eq. [35] is zero.) This implies that the overall timestep, τ_0, of the integrator should be small enough to resolve the perihelion passage of all the objects in the system for all times. This is a

limitation of the code that we are currently attempting to remove but we have thus far been unsuccessful.

(iii) For a very close encounter between two bodies i and j, the relative velocity between the two bodies roughly scales as $r_{ij}^{-1/2}$ at small r_{ij}. A scaling argument based on this assumption and equation (35) leads to the conclusion that the dominant energy error term scales as τ_k^2/r_{ij}^4 when $r_{ij} \sim R_k$. Therefore, a choice of the radii, R_k, of the shells at which the timestep is changed which satisfies the relationship $R_k/R_{k+1} = (\tau_k/\tau_{k+1})^{1/2}$ makes the energy error independent of separation.

We have implemented SyMBA in a computer code. For the remainder of this paper, we consider a SyMBA integrator with $M = \tau_k/\tau_{k+1} = 3$. We have found through experimentation that the the choice of the R_k's suggested in point iii above is computationally very expensive and is steeper than is necessary for all but the most extreme encounters. Since for most applications, objects suffer collisions before this steep scaling is necessary, we choose $R_k/R_{k+1} = 2.08$, which is equivalent to the timestep decreasing as $r_{ij}^{3/2}$. Finally, through experimentation, we found that R_1 should be ~ 3 mutual Hill radii.

6. Tests of SyMBA

Testing of a code such as our SyMBA integrator is a complicated task since it is intended to model chaotic systems, which do not have analytic solutions. There are no sample problems that we can run that test *all aspects* of the code against exact known solutions. Thus we pursued two separate avenues of approach to test our code: (*i*) The few special cases for which there are conserved quantities were used as tests. Unfortunately, such tests are somewhat limited. They either involve only global parameters (such as the conservation of energy), or require very simple planetary systems (such as the circular restricted 3-body problem). We ensure that the code conserves these quantities to high numerical accuracy in all problems of this type that are known to us. (*ii*) A suite of short time duration problems designed to test the SyMBA code was run using our code as well as several other well-established codes. We verified that the results from our code statistically agreed with the results from the established codes in each of these cases. We developed several tests for each of these categories. Overall, we carefully designed and implemented tests that exercised all aspects of the code. As an illustration, we now present the results of a few of these tests.

6.1. Binary Planets

As a very stringent test of our code, we integrated a pair of bound binary planets with their center of mass revolving about a star. The center of mass of the binary was placed in a 1 AU nearly circular orbit about a solar-mass star. The initial semi-major axis of the relative orbit of the binary was 0.0125 AU and the initial eccentricity was 0.6. Each planet had a mass of $10^{-3}\,M_{\odot}$, or about the mass of Jupiter. We integrated this system for 100 years (or about 3200 orbital periods of the binary) with a timestep of 0.01 years.

Figure 4 shows the results of this integration. The semi-major axis and eccentricity are well behaved. The energy error is small, usually less than 10^{-6}, although there is a slight systematic decrease over the length of the run. The separation between the binary planets ranges from 5×10^{-3} to 0.02 AU, which corresponds to k ranging from 4 to 6 in our recursion levels.

6.2. Scaled Outer Solar System

We integrated a solar system consisting of the Sun and four giant planets, with the masses of the planets increased by a factor of 50. We used a small timestep of 0.03 years because the planets were so massive. It is well known that such a system is unstable and

that the planets evolve onto crossing orbits on a short timescale (Duncan & Lissauer 1998). Figure 5 shows the behavior of the system as a function of time. Each planet is represented by a colored pair of curves: black, red, green, and blue represent Jupiter, Saturn, Uranus, and Neptune, respectively. The solid curves represent the planets' perihelion distances, while the dotted curves are their aphelion distances. Although the planets are initially on nearly circular orbits, their eccentricities quickly grow. At $t \sim 30$ years, the orbits of Neptune and Saturn become crossing, after which the evolution becomes violent. Saturn is ejected from the system 1920 years into the simulation, while Uranus quickly follows 60 years later.

Figure 6 shows the fractional change in the energy of the system as a function of time. Note that this value is fairly small. In addition, it seems to be oscillating around zero and does not show a systematic growth.

6.3. The Circular Restricted 3-Body Problem

We integrated the orbits of 50 massless test particles under the gravitational forces of the Sun and Neptune ($a = 30\,\mathrm{AU}$). Neptune was placed on a circular orbit. The initial semi-major axes of the test particles were uniformly distributed between 36 and 40 AU. Their initial inclinations were set at zero with respect to Neptune and their initial perihelion distances were 30 AU. The initial Jacobi constants of these particles were such that Neptune could not eject them from the solar system or allow them to impact the Sun since they must remain on Neptune-encountering orbits. We stopped the particles if they came within Neptune's physical radius. The timestep for the integration was 2 years.

The integration lasted for 10^9 years, although the median lifetime of the particles was 2.9×10^6 years. Over the integration, none of the particles were ejected from the system. The Jacobi constant was well conserved for all the particles. Indeed, the *worst case* was a variation of 1 part in 29,000.

6.4. Gravitation Focusing

Greenzweig & Lissauer (1990) performed a careful analysis of the enhancement of the collision cross-section of planets due to gravitational focusing. They integrated the orbits of millions of massless particles under the gravitational attraction of the Sun and a planet using a Bulirsch-Stoer integrator. The planet was on a circular orbit of 1 AU and had a mass of $10^{-6}\,M_\odot$. They performed several sets of runs. For each set, the particles initially had the same eccentricity and inclination, but had a range of semi-major axes. The inclination and

range of semi-major axis increased as the eccentricity increased (see Table 1 of Greenzweig & Lissauer 1990 for a complete description of the initial conditions). Since the particles in each set had a unique eccentricity, we identify each run by its eccentricity. All particles had semi-major axes very close to the planet and very small inclinations and eccentricities. Indeed, in the most extreme case we study here, the semi-major axis ranged from 0.977 to 1.023 AU, the eccentricity was ~ 0.007, and the inclination was 0.2°. In addition, the physical radius of the planet was chosen to be one of two values, $R_{\rm phy} = 0.1 R_H \approx 10^5$ km and $R_{\rm phy} = 0.005 R_H \approx 5200$ km, where R_H is the Hill radius of the planet.

The orbits of the test particles were integrated through one close encounter with the planet with a timestep of 5×10^{-3} years. The number of objects that impacted the planet was recorded. Figure 7 shows the fraction of objects that impacted as a function of eccentricity as reported by Greenzweig & Lissauer (1990) (open symbols, connected by curves) and as calculated by SyMBA (filled symbols). The squares and circles represent the two different values for the physical radius of the planet. Since we were limited in the number of particles whose trajectories we integrated, error bars are shown for the SyMBA results assuming Poisson statistics. As the figure shows, there is very good agreement between Greenzweig & Lissauer's results and those using SyMBA.

6.5. The Accretion of the Moon

Ida et al. (1997) used an Aarseth-type N-body code (Makino & Aarseth 1992) to study the accretion of the Moon after a giant impact. As a test of SyMBA, we have reproduced a simulation which is a forerunner of those which are reported in Ida et al. (1997). The units for this calculation were Earth mass, Roche radius, and $G = 1$. Thus an object with a semi-major axis at Earth's Roche radius, R_E, had an orbital period of 2π. The particles initially had masses that ranged from 3.2×10^{-7} to $3.2 \times 10^{-4} M_\oplus$, semi-major axes that ranged from 0.7 to 1.3 R_E, eccentricities that ranged from zero to 0.95, and inclinations that ranged from zero to 50°. Initially there were 999 particles in the simulation. Since the DH method does not handle orbits with small pericentric distances very well, we first removed the 9 objects that had initial pericentric distances less than the radius of the Earth.

As a test of energy conservation, we integrated the orbits of the bodies for three orbital periods (6π time-units) using a timestep of 0.2. We did not allow physical collisions in this simulation so that energy conservation could be checked. Note that the optical depth for gravitational scattering (using a cross section based on the Hill radius of the particles) is roughly 0.3 in this system, and many encounters happened during this short run. This experiment most effectively tests the ability of the code to handle a large number of simul-

taneous distant encounters. However, we estimate that encounters as close as 2% of mutual Hill radius (or about 4% of the physical radius) occurred during the simulation. Figure 8 shows that the energy is very well conserved.

We then used SyMBA to integrate this system for 10^3 orbital periods, this time allowing physical collisions. We assumed that a collision always led to a merger. The mass and the momentum of the merger product were calculated assuming that the total mass and momentum were conserved. This is somewhat different from the assumptions in the published paper by Ida et al. (1997), where they did not allow a merger between two objects if they filled their mutual Hill sphere. However, the run that they supplied us was one of their test cases where they employed the same assumptions that we did here. Figure 9 shows the number of bodies left in the simulation as a function of time. As can be seen from the figure, there is excellent agreement between our simulation and theirs.

7. Concluding Remarks

The development of the highly efficient computer algorithms known as Mixed Variable Symplectic (MVS) methods (Wisdom & Holman 1991) has allowed integrations of objects in the solar system on timescales equal to the age of the solar system for the first time. However, existing MVS integrators gain much of their speed advantage in cases in which the mutual forces among the orbiting bodies are small. Thus, they cannot both maintain their speed advantage and accurately handle a close encounter between two bodies.

We present a new symplectic algorithm that has the desirable properties of MVS methods, but can handle close encounters between massive bodies. This technique, known as the *Symplectic Massive Body Algorithm* or SyMBA, is based on a variant of the standard MVS method, with the Hamiltonian written in terms of heliocentric positions and barycentric momenta. SyMBA handles close encounters by employing an improved version of the multiple timestep technique proposed by Skeel & Biesiadecki (1994). When the bodies are well separated, the algorithm has the speed of the MVS method, but whenever two bodies suffer a mutual encounter, the timestep for the relevant bodies is recursively subdivided to whatever level is required. During the encounter, the algorithm is similar to a '$T+V$' symplectic leapfrog integrator. SyMBA is *symplectic* and *time reversible* and has a surrogate Hamiltonian that is well behaved.

Testing of a code such as our SyMBA integrator is a complicated task since it is intended to model chaotic systems, which do not have analytic solutions. We pursued two independent approaches to testing our code: (*i*) The few special cases for which there are conserved quantities (such as the energy or the Jacobi constant) were used as tests. (*ii*) Published (or about to be published) examples of more complex problems solved using other techniques were also used as tests. We developed several tests for each of these categories, five examples of which were presented above. In all we found that the code worked very well, as long as the pericentric distances did not get very small. Thus, we believe that SyMBA will be a valuable tool for the study of the late stages of planet formation.

We would like to thank M. Holman, G. Stewart, and S. Tremaine for useful discussions. We are also grateful to J. Chambers, S. Ida, and G. Wetherill for comparison problems. SyMBA was developed, in part, under a SwRI internal research grant. HFL is grateful to NASA's Exobiology, PGG, Origins, programs for funding. MJD is grateful for the continuing financial support of the Natural Science and Engineering Research Council. MHL is grateful for a CITA National Fellowship.

REFERENCES

Biesiadecki, J. J., & Skeel, R. D. 1993, J. Comput. Phys., 109, 318

Chambers, J. E., & Wetherill, G. W. 1998, Icarus, submitted

Duncan, M. J., Levison, H. F., & Budd, S. M. 1995, AJ, 110, 3073

Duncan, M. J., & Lissauer, J. J. 1997, Icarus, 125, 1

Duncan, M. J., & Lissauer, J. J. 1998, Icarus, submitted

Forest, E., & Ruth, R. D. 1990, Physica D, 43, 105

Greenzweig, Y., & Lissauer, J. J. 1990, Icarus, 87, 40

Holman, M. J., & Wisdom, J. 1993, AJ, 105, 1987

Ida, S., Canup, R. M., & Stewart, G. R. 1997, Nature, 389, 353

Lee, M. H., Duncan, M. J., & Levison, H. F. 1997, in Computational Astrophysics, Proc. 12th Kingston Meeting, ed. D. A. Clarke & M. J. West (San Francisco: ASP), 32

Levison, H.F., Duncan, M. 1994, Icarus, 108, 18.

Makino, J., & Aarseth, S. J. 1992, PASJ, 44, 141

Ruth, R. D. 1983, IEEE Trans. Nucl. Sci., 30, 2669

Saha, P., & Tremaine, S. 1992, AJ, 104, 1633

Saha, P., & Tremaine, S. 1994, AJ, 108, 1962

Sanz-Serna, J. M., & Calvo, M. P. 1994, Numerical Hamiltonian Problems (London: Chapman & Hall)

Skeel, R. D., & Biesiadecki, J. J. 1994, Ann. Numer. Math., 1, 191

Skeel, R. D., & Gear, C. W. 1992, Physica D, 60, 311.

Szebehely, V. 1967, Theory of Orbits (New York: Academic)

Touma, J., & Wisdom, J. 1994, AJ, 107, 1189

Wisdom, J., & Holman, M. 1991, AJ, 102, 1528 (WH91)

Yoshida, H. 1990, Phys. Lett. A, 150, 262

Yoshida, H. 1993, Celest. Mech. & Dyn. Astr., 56, 27

Fig. 1.— The decomposition of the force $F(r) = 1/r^2$ into its components, F_i. Components $i = 0$ through 3 are shown, with $R_1 = 1$ and $R_i/R_{i+1} = \sqrt{2}$.

Fig. 2.— The fractional change in energy as a function of time for an integration of the four giant planets with a timestep of 0.4 years. Notice that the energy error is bounded as a result of the fact that there is a well behaved surrogate Hamiltonian for the integrations. **TOP:** The integration used the MVS integrator (Wisdom & Holman 1991). **BOTTOM:** The integration used the Democratic Heliocentric scheme developed here.

Fig. 3.— **TOP:** The maximum fractional change in energy for an integration of a system containing only the Sun and Jupiter as a function of Jupiter's perihelion distance. The Democratic Heliocentric (DH) scheme was used. **BOTTOM:** The maximum fractional change in energy for an integration of a system containing only the Sun, Jupiter, and Saturn as a function of Saturn's perihelion distance. Jupiter's initial eccentricity was 0.05 for all the runs. The solid and dashed curves refer to results obtained by the DH and the MVS scheme, respectively.

Fig. 4.— The dynamical behavior of a binary planet in a nearly circular heliocentric orbit at 1 AU. The mass of each planet is $10^{-3}\,M_\odot$. The TOP and CENTER panels shows the relative semi-major axis and eccentricity of the binary orbit, respectively. The BOTTOM panel plots the fractional change in total energy of the system.

Fig. 5.— The behavior of a system containing the Sun and four giant planets, where the mass of the planets has been increased by a factor of 50. Each pair of color curves represent the perihelion distance (solid curve) and aphelion distance (dotted curve) of a planet as a function of time. Black, red, green, and blue refer to Jupiter, Saturn, Uranus, and Neptune, respectively.

Fig. 6.— The fractional change in energy for the system whose behavior is shown in Figure 5.

Fig. 7.— The fraction of test particles that impacts a planet with a physical radius, $r_{\rm phy}$, as a function of the initial eccentricity of the test particles. The open symbols and curves show the results from Greenzweig & Lissauer (1990). Two sets of runs were performed. The first had $r_{\rm phy}$ of 0.1 of the planet's Hill radius (R_H) and is represented in the figure by the dotted curve and the squares. The second had $r_{\rm phy} = 0.005\,R_H$ and is represented by the solid curve and the circles. The filled symbols represent the results for the same runs using SyMBA. Since we were limited in the number of particles whose trajectories we followed, error bars are shown for the SyMBA results assuming Poisson statistics.

Fig. 8.— The fractional change in total energy for an integration using SyMBA of 990 proto-lunar objects in Earth orbit. See text for a description of the initial conditions. No physical collisions were allowed, so energy should be conserved. An object with a semi-major axis at Earth's Roche radius had an orbital period of 2π in the time units used in the figure.

Fig. 9.— The number of objects remaining in a simulation of the accretion of the moon as a function of time. The dots show the results from Ida et al. (1997), while the curve shows the results from the same simulation using SyMBA.

Figure1 —

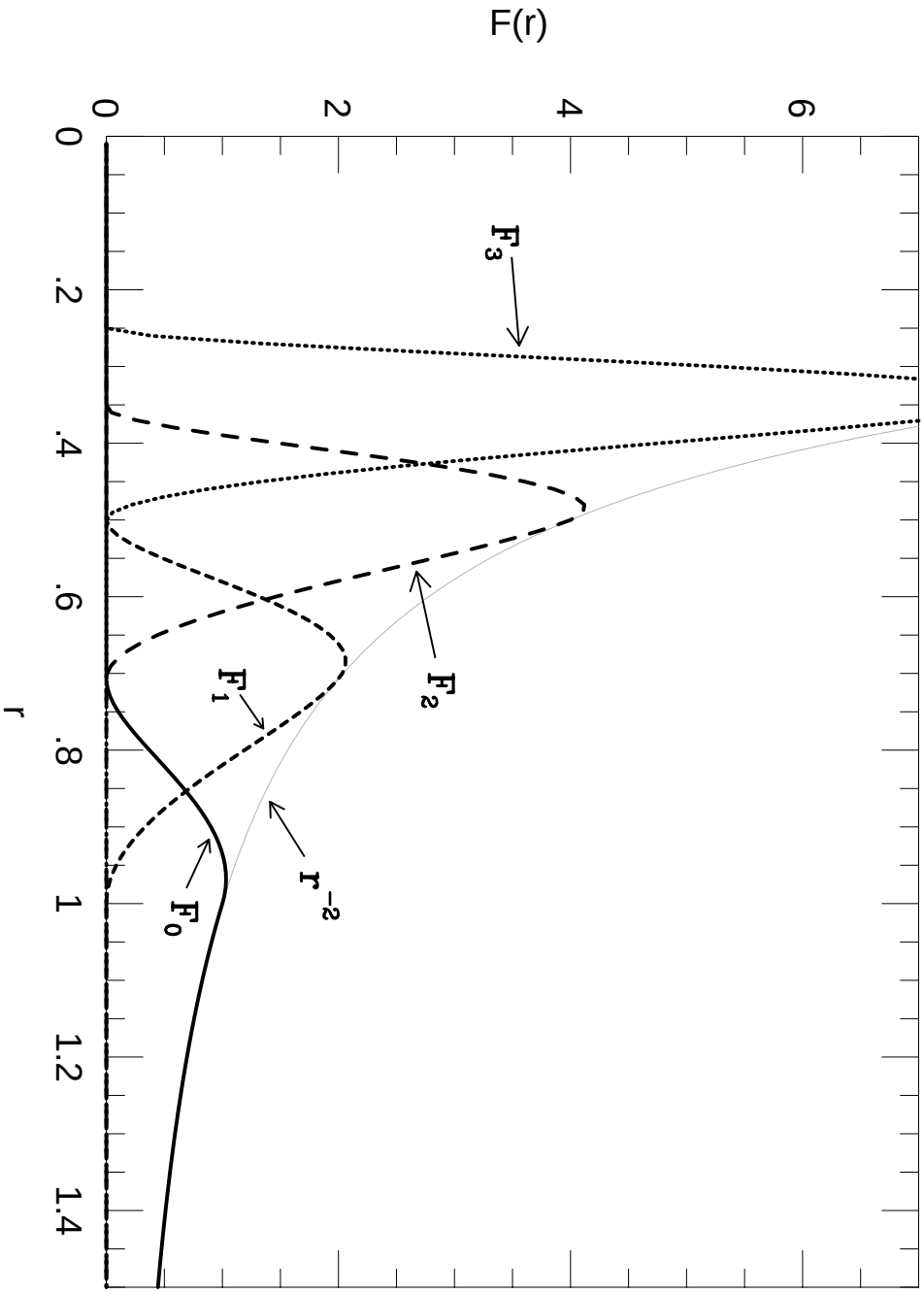

Figure2 —

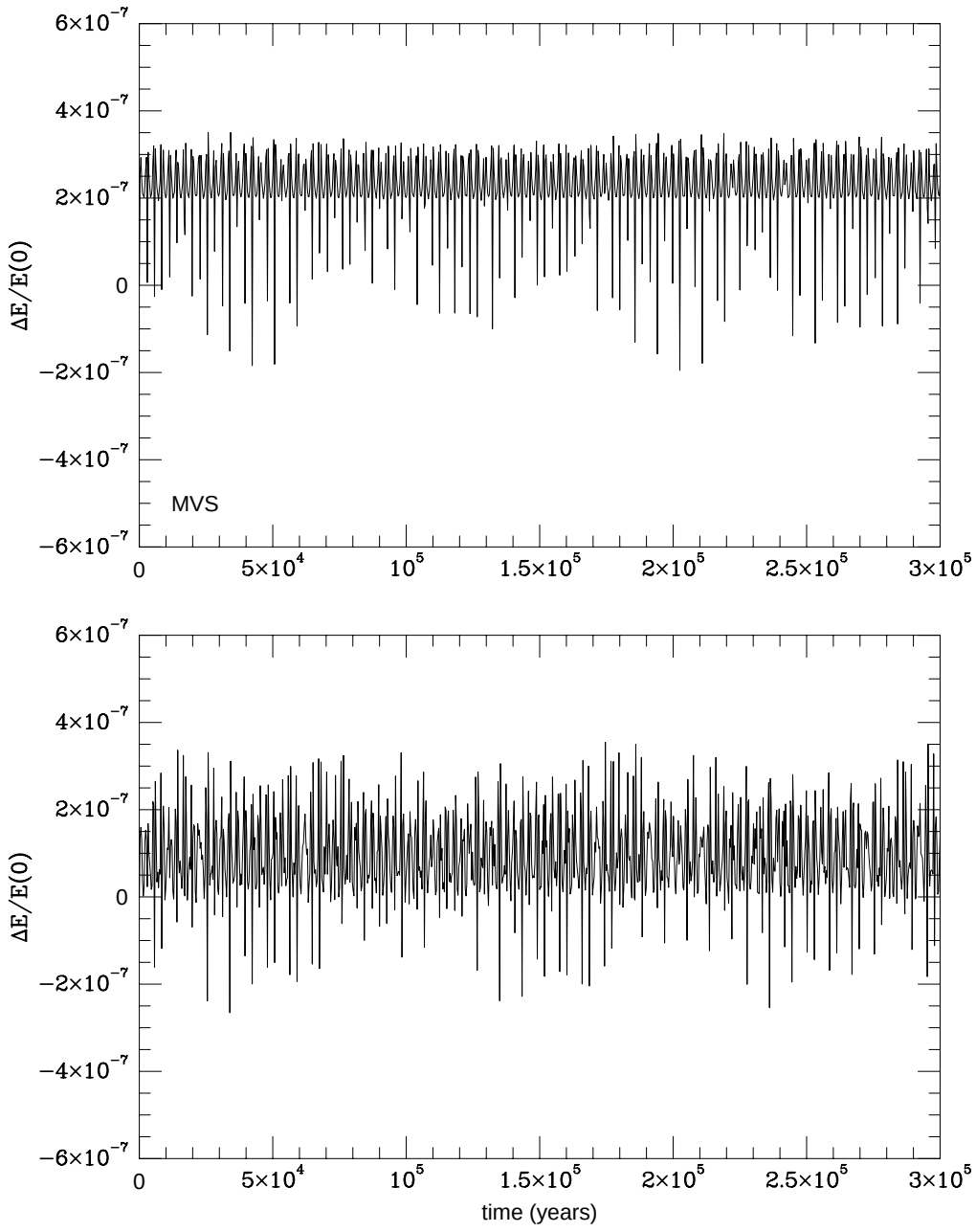
6×10⁻⁷
4×10⁻⁷
2×10⁻⁷
0
−2×10⁻⁷
−4×10⁻⁷
−6×10⁻⁷
ΔE/E(0)
MVS
0
5×10⁴
10⁵
1.5×10⁵
2×10⁵
2.5×10⁵
3×10⁵
time (years)

Figure3 —

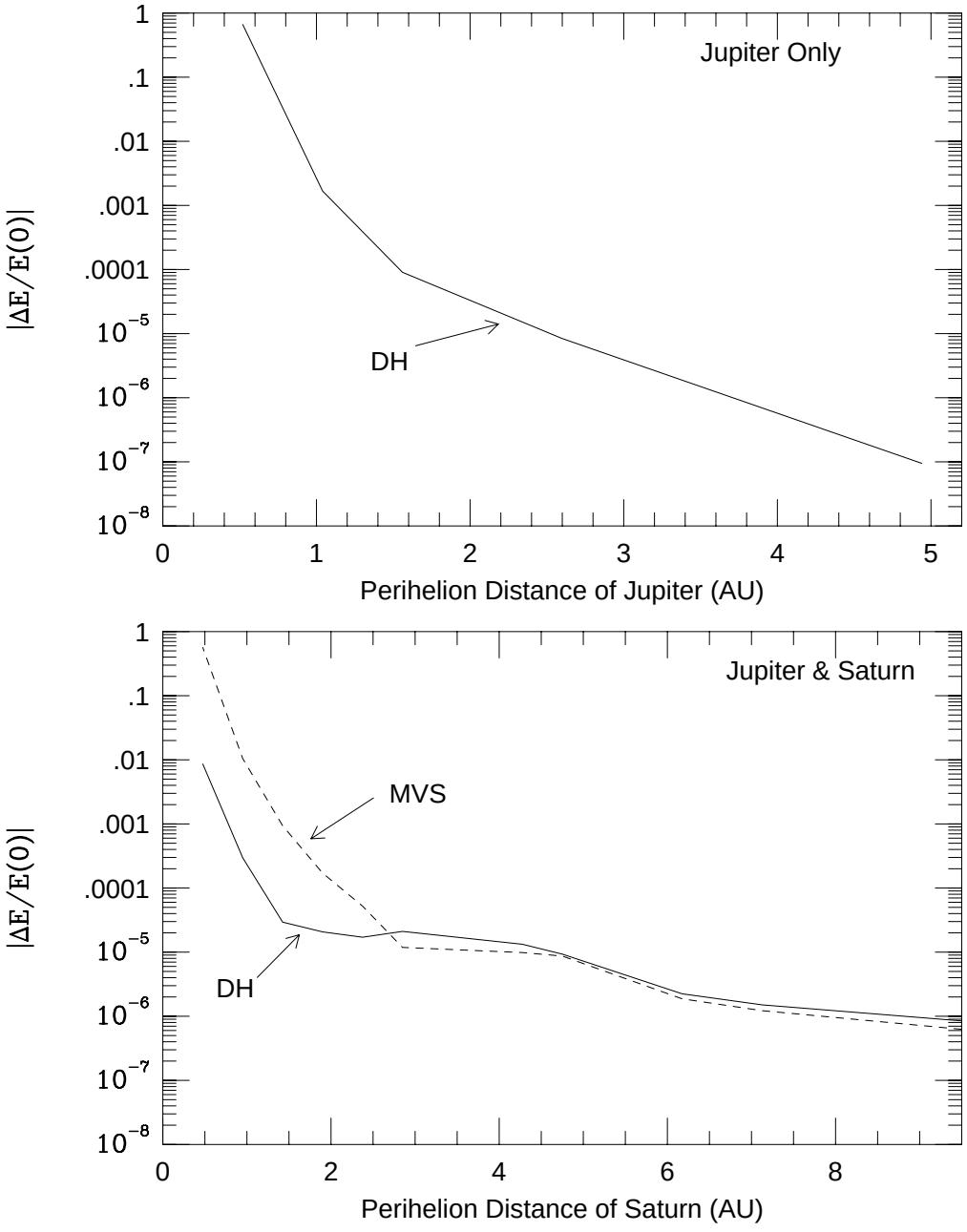
Jupiter Only
DH
|ΔE/E(0)|
Perihelion Distance of Jupiter (AU)
Jupiter & Saturn
MVS
DH
|ΔE/E(0)|
Perihelion Distance of Saturn (AU)

Figure4 —

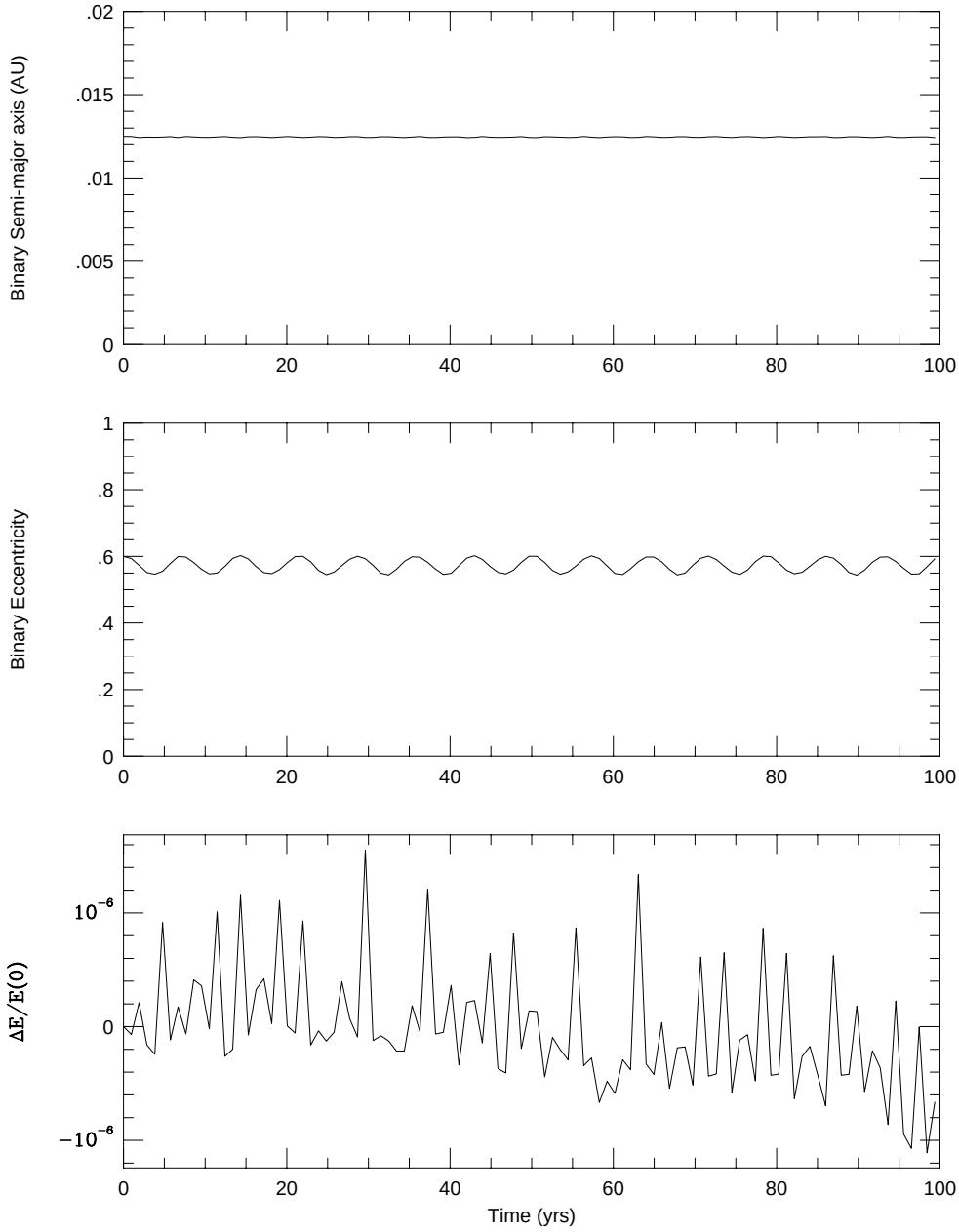
Binary Semi-major axis (AU)
.02
.015
.01
.005
0
0
20
40
60
80
100
Binary Eccentricity
1
.8
.6
.4
.2
0
0
20
40
60
80
100
ΔE/E(0)
10⁻⁶
0
−10⁻⁶
0
20
40
60
80
100
Time (yrs)

Figure5 —

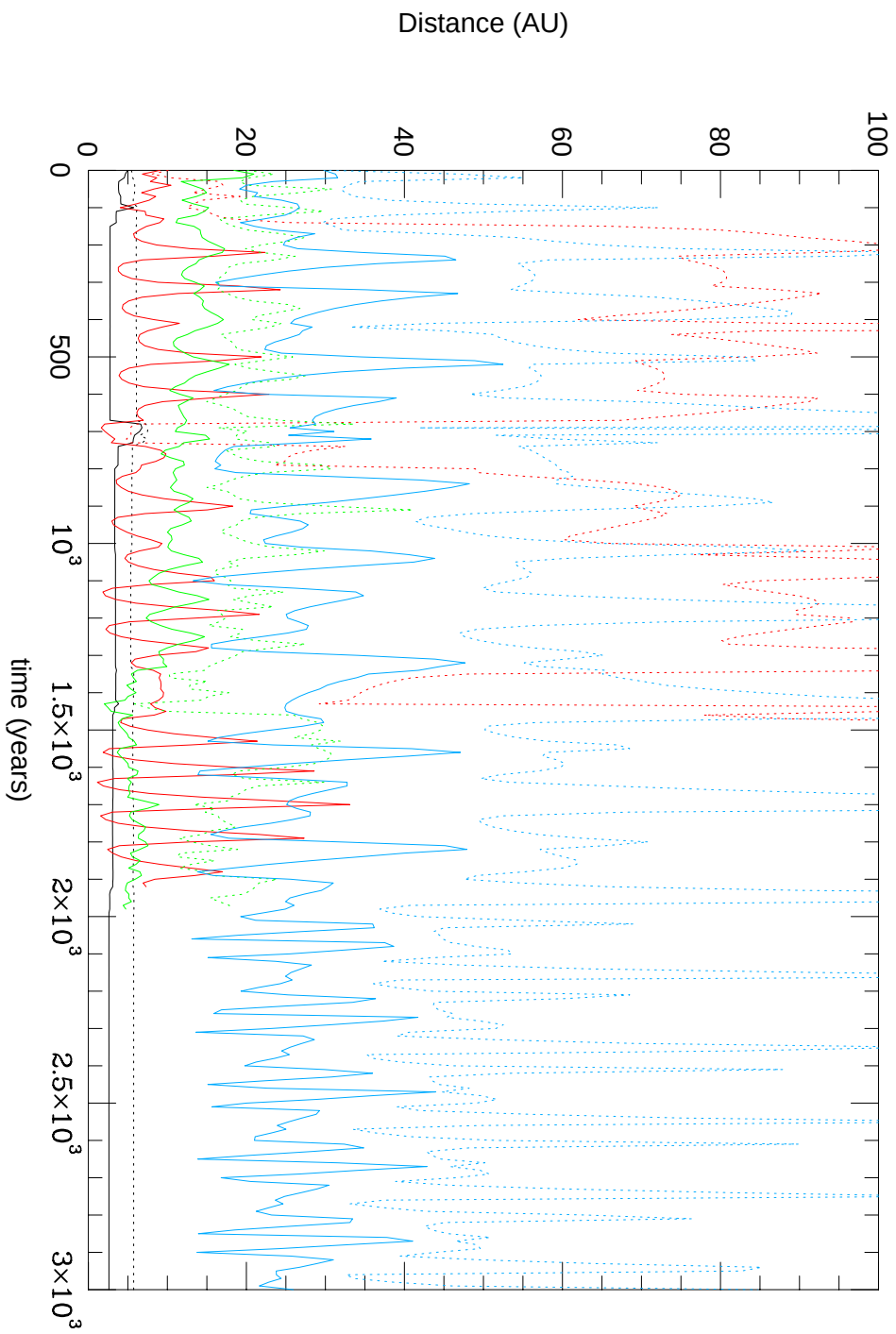
Distance (AU)
0
20
40
60
80
100
time (years)
0
500
10^3
1.5×10^3
2×10^3
2.5×10^3
3×10^3

Figure6 —

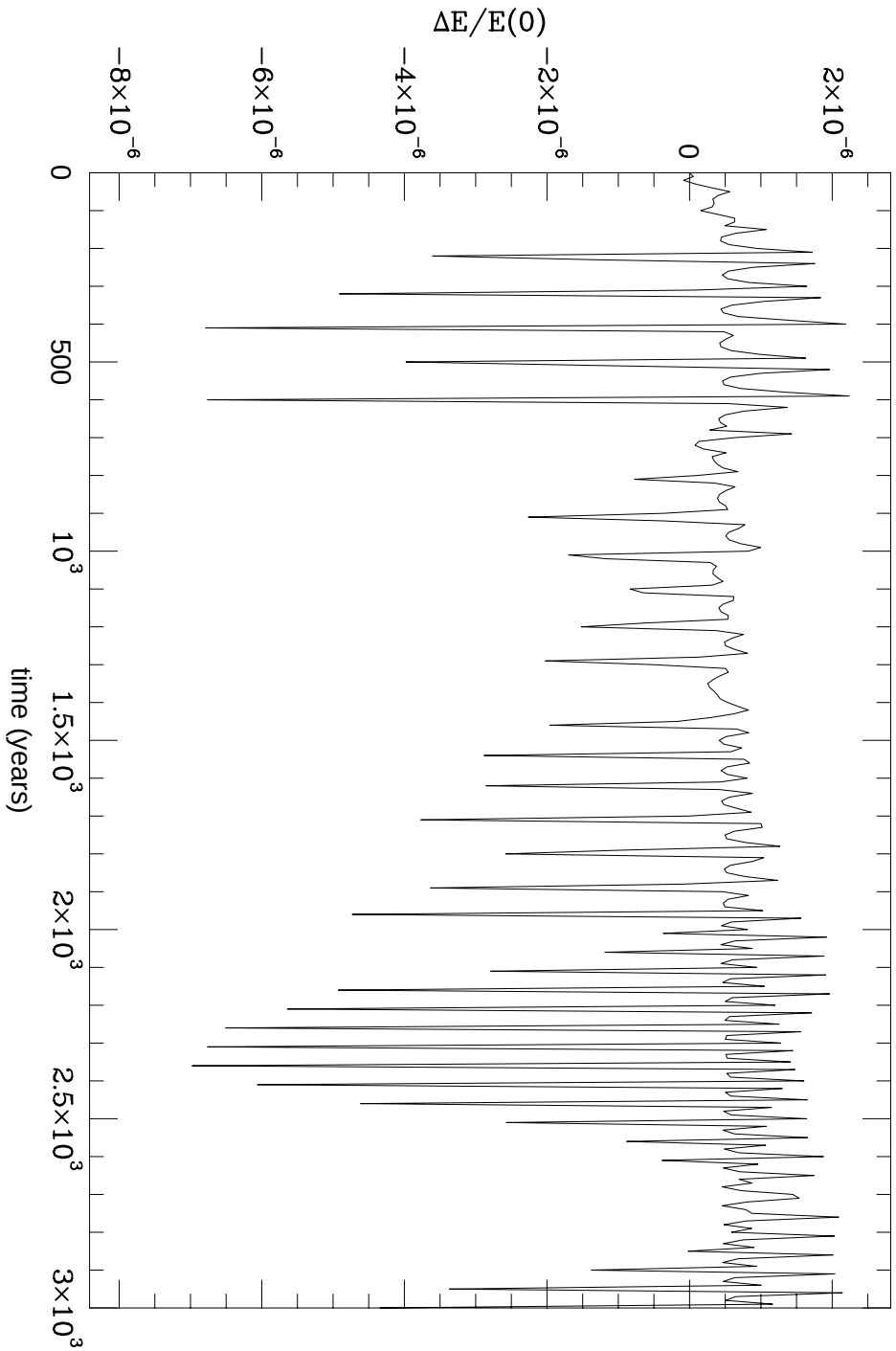
ΔE/E(0)
−8×10⁻⁶
−6×10⁻⁶
−4×10⁻⁶
−2×10⁻⁶
0
2×10⁻⁶
0
500
10³
1.5×10³
2×10³
2.5×10³
3×10³
time (years)

Figure7 —

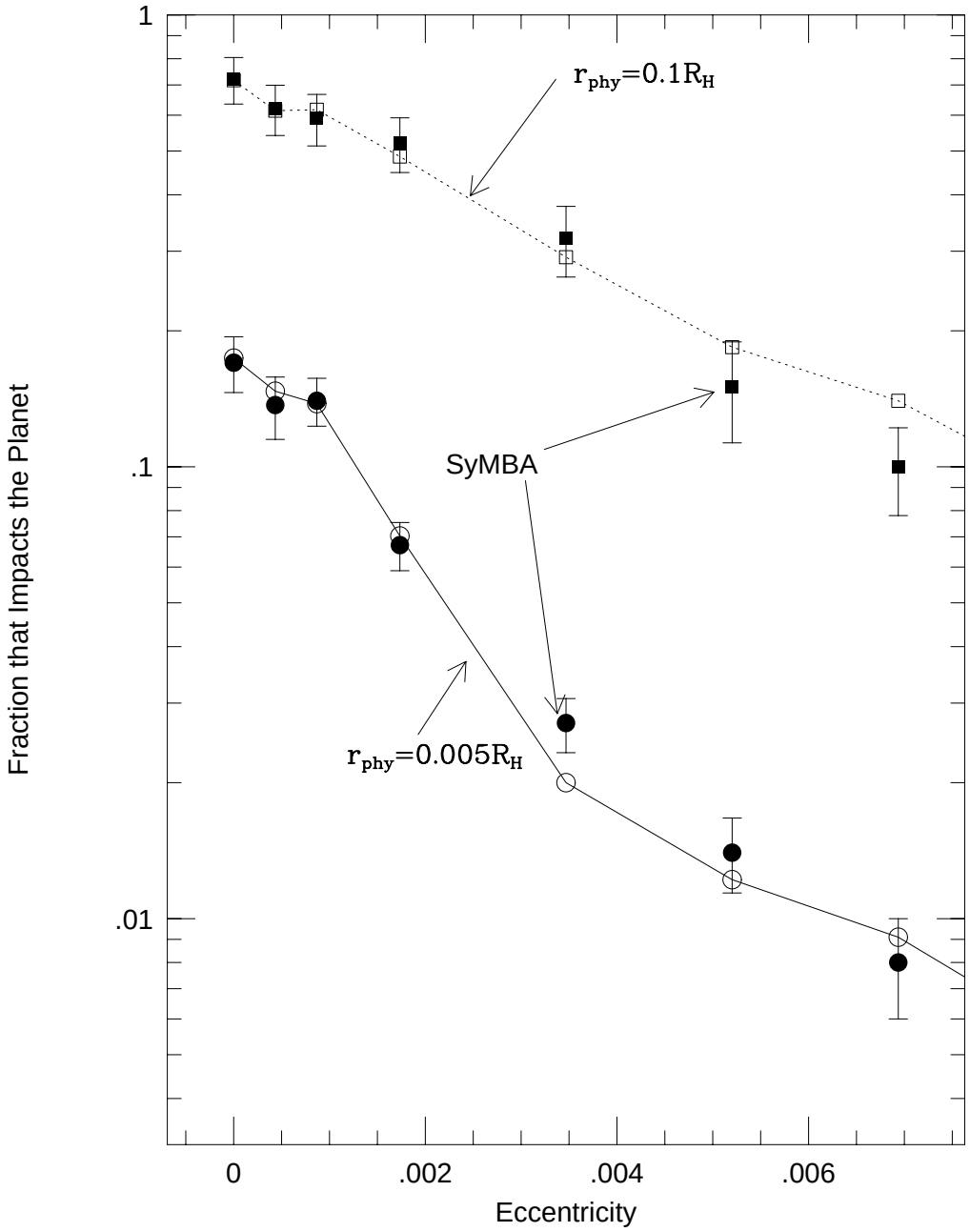
1
.1
.01
0
.002
.004
.006
Eccentricity
Fraction that Impacts the Planet
r_{phy}=0.1R_H
SyMBA
r_{phy}=0.005R_H

Figure8 —

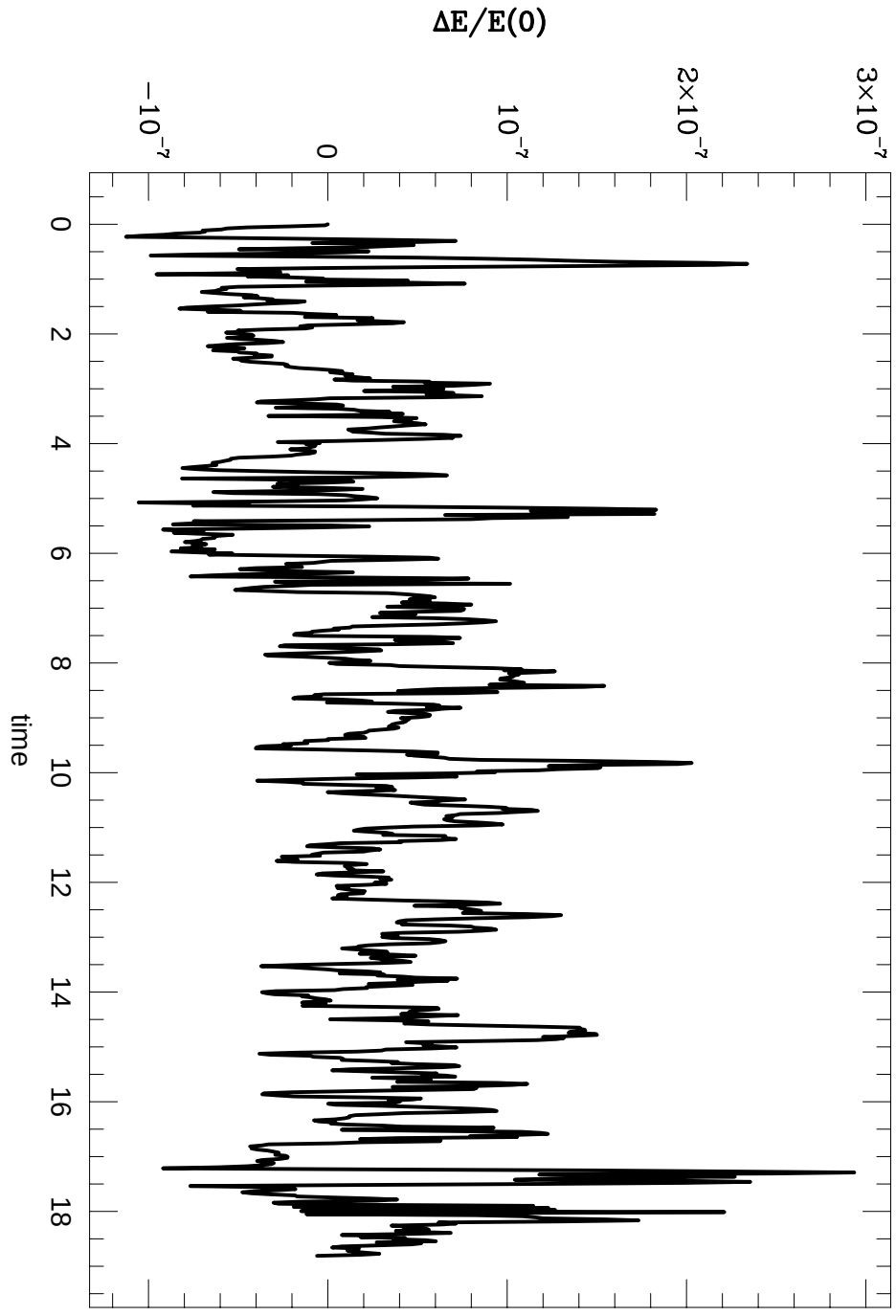

Figure9 —